MECSOL 2022 - Proceedings of the 8th International Symposium on Solid Mechanics
M.L. Bittencourt, J. Labaki, L.C.M. Vieira Jr. and E. Mesquita (Editors), Campinas SP, Brazil, October 17th to 19th, 2022

An implementation of 3D RVE-based computational homogenization considering an elastic-perfectly plastic matrix and spherical voids

Carlos Alberto da Maia[1], Andrey Brezolin[1], Tiago dos Santos[2] and Rodrigo Rossi[1]

[1] Departamento de Engenharia Mecânica, Universidade Federal do Rio Grande do Sul, R. Sarmento Leite,425, Porto Alegre, RS, Brazil

[2] Departamento de Engenharia Mecânica, Universidade Federal de Santa Maria, Av. Roraima, 1000, Prédio 7, Santa Maria, RS 97105-900, Brazil

Abstract: This work investigates the strength of porous materials using a finite element homogenization procedure based on three-dimensional Representative Volume Elements (RVE). The RVE consists of an aggregate composed of randomly distributed non-overlapping spherical voids embedded in an elastic-perfectly plastic matrix, obeying the von Mises criterion. In order to obtain distinct macroscopic stress states, mixed boundary conditions are imposed on the RVE. Using such conditions, it is possible to reach different macroscopic stress triaxialities by varying specific loading parameters. The macroscopic stress tensor is considered to be the average of its microscopic counterpart taken for a stabilized RVE response, which is found in terms of an asymptotic homogenized response. The calculations were carried out using the commercial finite element software Abaqus and the results were post-processed using a Python script, which calculates the stress averages based on information taken at each integration point in the RVE. The simulations are performed employing different initial void volume fractions using multiple pores and single pores, with different boundary conditions, which provide distinct macroscopic stress states. The obtained numerical results allow constructing macroscopic yield surfaces in the deviatoric-hydrostatic stress space depending on the initial void volume fraction and to compare the difference between multiple and single pores in an RVE with in same void volume fraction. The results showed that, for a low void volume fraction, a single pore can represent well a multiple pore model, while for larger void volume fractions, a single pore model presents deviations. The results were also compared with the Gurson and Gurson-Tvergaard-Needleman (GTN) models. It was noted that the Gurson model overestimates the results, while the results of the (GTN) model were close to the computational calculation.

Keywords: plasticity, representative volume element (RVE), computational homogenization, porous metals

INTRODUCTION

When thinking about possible defects such as pores in materials used to build structures such as cars, buildings, bridges, and airplanes, doubts regarding their effects on strength arise. However, porous materials can be designed with function of upgrad a product, customizing the material and improving structural components. Regarding the type of pores, they can be divided into materials with closed pores, used as structural impact absorber parts, or open pores, which find application where fluid transport is necessary, such as filtration, catalyst support, thermal, and acoustic insulation, deposit of lubricant, among others (Binder C. et al., 2013). Materials with closed pores can be produced in an uncontrolled way, having some undesired pores, as by additive manufacturing and laser melting (Ahmed Obeidi et al., 2021). Porous materials are sensitive to hydrostatic pressure and the analysis of hydrostatic pressure dependence of these materials can be taken into consideration for the designing of engineering materials. Green (1972) presented a theory of plasticity for porous solids, where the material is isotropic, and the pores are treated as voids. In the same way as Kuhn and Downey (1971), Green (1972) presented the yield criterion as a function of the first invariant of the stress tensor and the second invariant of the deviatoric stress tensor. The model proposed by Gurson (1977) can simulate the nucleation and growth of microvoids and is widely used. Tvergaard and Needleman (1984) improved the Gurson (1977) model by incorporating a damage nucleation mechanism into the Gurson model equation, in which voids are nucleated depending on the deformation history. The yield function of Tvergaard and Needleman (1984) is an empiric extension of the Gurson model, by introducing three more coefficients. Tvergaard and Needleman's model, also known as the GTN, has been used in several applications. However, the use of these plasticity models in porous materials do not consider the pore morphology, which deviates the mechanical behavior response in a real situation, not predicting the realistic behavior of the material.

In recent decades, many numerical analyzes have been performed two-dimensionally, which, in contrast to many structural problems, is relatively meaningless in mechanics real world applications (Zohdi and Wriggers, 2004). For a

statistically representative sample of microstructural material, three-dimensional numerical simulations are inevitable for reliable results. The contributions that gave rise to the current concept of multiscale models are not recent, as seen in Zaitsev and Wittmann (1981), where the authors simulate the propagation of cracks in concrete in multiscale systems based on representative volume element (RVE), obtaining satisfactory results. In Zhang and Harding (1990), a homogenization method for a composite fabric is presented, where the authors extract the homogenized properties of the material. In Guedes and Kikuchi (1990) the authors present a homogenization method for a material with a periodic microstructure and extract the elastic properties of the material. It is a pioneer work due to discussing the computational homogenization method for three-dimensional models. The authors determine the effective mean elastic constants of the linear elasticity of general composite materials by the adaptive finite element method. Guedes and Kikuchi (1990) also presented a study of convergence for a two-dimensional model providing results compatible with the error estimates. Regarding the use of 3D RVE based computational homogenization, one cites the work of Fritzen et al. (2012). The authors investigate the effective response of ductile metals containing pores by representing the pores in a three-dimensional RVE where the matrix was assumed as an elastic-perfectly plastic matrix, obeying von Mises criterion. Results are presented in the deviatoric-hydrostatic space and a comparison with the GTN model is provided. Following the same ideas, Fritzen et al. (2013) compared and proposed improvements for the yield function of Green (1972).

This work aims at modeling the strength of porous materials using a finite element homogenization procedure based on three-dimensional RVEs. The idea here is to follow the rationale of the work of Fritzen et al. (2012) while presenting details as how it is implemented inside the commercial software Abaqus showing aspects of pre and postprocessing, for which a Python Script is used to calculate the average values. However, while Fritzen et al. (2012) uses the analytical model of GTN, in this work we use the numerical model already implemented in the commercial software Abaqus and, using parameters of yield criterion of different references, arrive at a representation of the best GTN model which complies to the homogenized numerical results. We also present a study for multiple pores and single pores for all evaluated microstructures.

Modeling

In order to investigate the pressure dependence of the yielding of the three-dimensional microstructures on a computational basis, in this work we investigated the effective response of ductile material containing void volume fractions of 0.1%, 1%, 2.5%, 5%, 10%, 20% and 30%. Periodic aggregates (meso-scale level) made up of a homogeneous material matrix are considered. The periodicity of the pore distribution was guaranteed using Mote3D (Richter, 2017). A single pore embedded in the RVE was also used in the study as reference and for sake of comparison of results.

It was considered to use a perfectly plastic model, with constant yield stress σ_F=100 MPa, with the material being isotropic and following the von Mises criterion. For the elastic part, the material parameters are Young's modulus E=200 GPa and Poisson's ratio ν=0.3. The pores are modeled as one-size-fits-all non-overlapping spherical voids, randomly distributed and without pressure. Since the matrix material is elastic perfectly plastic, the associated yield surface remains fixed regardless of any deformation process that the material may undergo.

Computational Homogenization

The homogenization method consists of calculating the volume average of key quantities such as the stress components while imposing strain boundary conditions along the RVE volume. Homogenization is performed with respect to the domain in the reference configuration. The disturbance of the RVE equilibrium is defined by the macroscopic deformation. The finite element implementation for the homogenization problem requires performing the RVE discretization. The ABAQUS software has an output field where the user can choose the *IVOL* option, which is the volume of the integration point, that is, associated with each Gauss point of the element, which is used in the numerical integration. Thus, for an RVE with or without voids, the averages can be represented by

$$\Sigma_{ij} = \frac{1}{V_{RVE}} \sum_{\xi=1}^{n} \left[\sigma_{ij}\left(\xi\right) \right] \times IVOL\left(\xi\right), \tag{1}$$

where ξ represents the point of integration and V_{RVE} the volume of the RVE (external edges) and σ_{ij} is micro stress. The solution of Eq. (1) comes from the approximation of the RVE geometry by discretization, in this way the precision of the calculation depends on the FE mesh. In this work, the *IVOL* is requested for the RVE in the reference state, while the micro stress σ_{ij} is requested for the RVE in the updated state.

Boundary Condition

To evaluate the yield surface, variable stress triaxiality must be induced. For this purpose, mixed periodic boundary conditions are used. Alternative loading conditions are often used to control the triaxiality ratio during loading, as seen in Besson et al. (2004), Fritzen (2012), Fritzen (2013) and Khdir et al (2014). A variable general triaxiality results from the prescription of the real value parameters α and β. For a time t, the following nominal strains are imposed on the RVE, while ensuring that they are free of shear stresses

$$\left.\begin{aligned}\bar{\varepsilon}_{11}(t) &= t\dot{\varepsilon}_0(\alpha+\beta)\\ \bar{\varepsilon}_{22}(t) &= t\dot{\varepsilon}_0(-\alpha+\beta)\\ \bar{\varepsilon}_{33}(t) &= t\dot{\varepsilon}_0\beta\end{aligned}\right\}, \tag{2}$$

where $\dot{\varepsilon}_0$ is a prescribed reference rate of deformation and α and β are loading parameters in order to obtain distinct stress triaxiality, different values are set to α and β. The values used in the analysis are given in Tab. 1. If a smoother yield surface is required Tab. 2 presents 20 loading cases to be applied in Eq. (2).

Table 1 – 9 loading cases

Case	1	2	3	4	5	6	7	8	9
α	1	1	1	1	1	1	1	0.5	0
β	0	0.5	0.1	0.15	0.25	0.5	1	1	1

Table 2 – 20 loading cases

Case	1	2	3	4	5	6	7	8	9	10	11	12	13	14	15	16	17	18	19	20
α	1	1	1	1	1	1	1	1	1	1	0.7	0.5	0.3	0.25	0.2	0.15	0.1	0.05	0.025	0
β	0	0.1	0.2	0.3	0.4	0.5	0.6	0.7	0.8	0.9	1	1	1	1	1	1	1	1	1	1

The deformation proceeds until reaching an asymptotic macroscopic stress state (see Fritzen (2012)). Next, the macroscopic stress components are calculated using Eq. (1). Then, the macroscopic von Mises equivalent stress and the macroscopic hydrostatic stress are respectively calculated

$$\begin{aligned} q &= \sqrt{\frac{3}{2}}\left\|\Sigma'_{ij}\right\|_2 = \sqrt{\frac{\left(\Sigma_{xx}-\Sigma_{yy}\right)^2+\left(\Sigma_{xx}-\Sigma_{zz}\right)^2+\left(\Sigma_{yy}-\Sigma_{zz}\right)^2}{2}}\\ p &= \frac{\mathrm{tr}\left(\Sigma_{ij}\right)}{3} = \frac{\Sigma_{xx}+\Sigma_{yy}+\Sigma_{zz}}{3}\end{aligned}, \tag{3}$$

where Σ_{xx}, Σ_{yy} and Σ_{zz} are the macro stress in the x, y and z directions, respectively.

Discretization and Mesh Convergence Analysis

Second-order tetrahedral elements with 10 nodes were used to discretize the RVE matrix. To show the convergence with respect to the element size and in order to investigate the error with relation to the finite dimensional approximation space, a mesh convergence study was carried out based on a model containing 105 pores and 30% of porosity. Nine different levels of discretization were considered, see Tab. 3. In order to guarantee a sufficient quality of the results presented with regard to the solution, a convergence study was carried out in a unit cell for the parameters f = 30%, N = 105 for the principal stress, von Mises stress and hydrostatic components. Load case 9 (α=0, β=1 in Tab. 1) was chosen as an example. Also, the discretization with the highest number of elements was taken as a reference solution and the response of all other discretization is related to the last calculated value of this discretization.

Table 3 – Mesh Refinement

Refinement	h_1	h_2	h_3	h_4	h_5	h_6	h_7	h_8	h_9
n° elements	25,853	50,172	73,367	100,592	149,102	205,579	249,944	299,909	858,266

Representativeness

In the considered continuum structure, there is no length scale in the assigned RVE. Thus, the unit cell size is given by the number of pores N, which must be chosen to be large enough to ensure that the RVE is representative. For more details, see Huet (1990), Drugan and Willis (1996) and Kanit et al. (2003), in which they study how the mechanical response depends on the size of the RVE.

In order to examine the influence of representativeness, a new set of random microstructures was created for porosity f = 30% and variable number of pores (N = 1, 5, 21, 44, 70, 105, 126, 150, 162, 200). All these microstructures are subjected to loading 5 (α=1, β=0.25 in Tab. 1), because it enforces both pronounced hydrostatic and deviatoric stress

components. To guarantee the independence of fluctuations with respect to the chosen spatial discretization, very refined meshes are used, above 300,000 elements. Of the 10 simulations with 10 different microstructures with different levels of porosity, N=105 was chosen, as it presents the smallest error associated with von Mises and hydrostatic stress as a function of the average of the 10 models. To verify the discrepancy between the construction of the randomness of the pores of the RVEs with the Mote3D (Richter, 2017), 7 simulations were also carried out with 7 different random microstructures, containing 105 pores each. In addition, to show that there is no length scale tied to the RVE size,14 more simulations were performed, all with 105 pores and with the same pore distribution, but with a scale ranging from 0.25 to 10 times (scale=0.25, 0.6, 0.8, 0.9, 1, 1.25, 1.5, 1.75, 2, 3, 4, 5, 6 and 10) of the RVE volume. It was considered to use the same mesh for all these models and the same strain level.

Gurson-Tvergaard-Needleman model

To improve the Gurson model, a damage nucleation mechanism in which voids are nucleated depending on the deformation history, was proposed by Tvergaard and Needleman (1984). The yield function Φ is a modification of the Gurson model and is represented by

$$\Phi = \left(\frac{q}{\sigma_F} \right)^2 + 2q_1 f^* \cosh\left[\frac{3q_2 p}{2\sigma_F} \right] - 1 - q_3 f^{*2} = 0, \tag{4}$$

where f^* is an effect that considers the interaction between the pores (see Tvergaard and Needleman (1984)). When the pores reach a certain volume, there is a decrease of the load capacity of the material. q_1, q_2, and q_3 are coefficients of the void volume fraction in terms of pressure. Notice that defining $q_1 = q_2 = q_3 = 1$ in Eq. (4) the original Gurson model is recovered. Table 4 shows some studies where researchers vary q_1, q_2, and q_3. For the numerical model of GTN and Gurson, it was decided to use the model already implemented in the Abaqus software, the Porous Metal Plasticity tool (Abaqus, 2022), and to compare it with the computational homogenization model to check which reference (Tab. 4) best approximates the numerical results, in addition to evaluating the loading history.

Table 4 – Values q_1, q_2 and q_3 for GTN equation

Reference	q_1	q_2	q_3
Gurson, 1977	1	1	q_1^2
Tvergaard, 1982	1.5	1	q_1^2
Koplik and Needleman, 1988	1.25	1	q_1^2
Zuo et al., 1996	1.4	1	q_1^2
Faleskog et al., 1998	1.46	0.93	q_1^2
Zhang et al., 2000	1.25	1	q_1^2
Nègre et al., 2003	1.5	1.2	q_1^2
Kim et al., 2004	2	0.909	q_1^2
McElwain et al., 2006	1.31	1.16	q_1^2
Nielsen and Tvergaard, 2009	2	1	q_1^2
Dunand and Mohr, 2011	1	0.7	q_1^2
Yan et al., 2013	1.55	0.9	q_1^2

RESULTS

The results presented in Fig. 1 show the yield surface for the multiple pores and single-pore computational homogenization models in *q-p* space, for various porosity levels where, "A" and "B" in the legend represent single-pore and multi-pore microstructures, respectively. Below the legend the RVE drawings are presented to give an idea of the porosity dimension/distribution considered. The asymptotic behavior is plotted in the *q-p* stress space for all microstructures examined and all nine loading directions considered. The computed data were used to compare with the Gurson and GTN model from Abaqus. It is notable that the yield surface decreases with increasing porosity, this is due to the RVE having a smaller matrix volume fraction, causing yielding to occur earlier than if the material were totally dense. And in the case of several pores, there is still the interaction between neighboring pores, further intensifying the beginning of yielding.

The graph presented in Fig. 2a) shows the yield surface in the *p-q-f* space where the blue curves are the yield surfaces for each level of porosity and the green curves represent the connections of the load cases of Tab. 2 evaluated between the porosity levels, thus characterizing a 3D surface in the *p-q-f* space. The Fig. 2a) also helps in the experimental (or numerical) evaluation of the yield of porous materials, without the need to perform numerical implementation and, using

a linear interpolation between the different porosity values, the test point can be located, characterizing the elastic or plastic state.

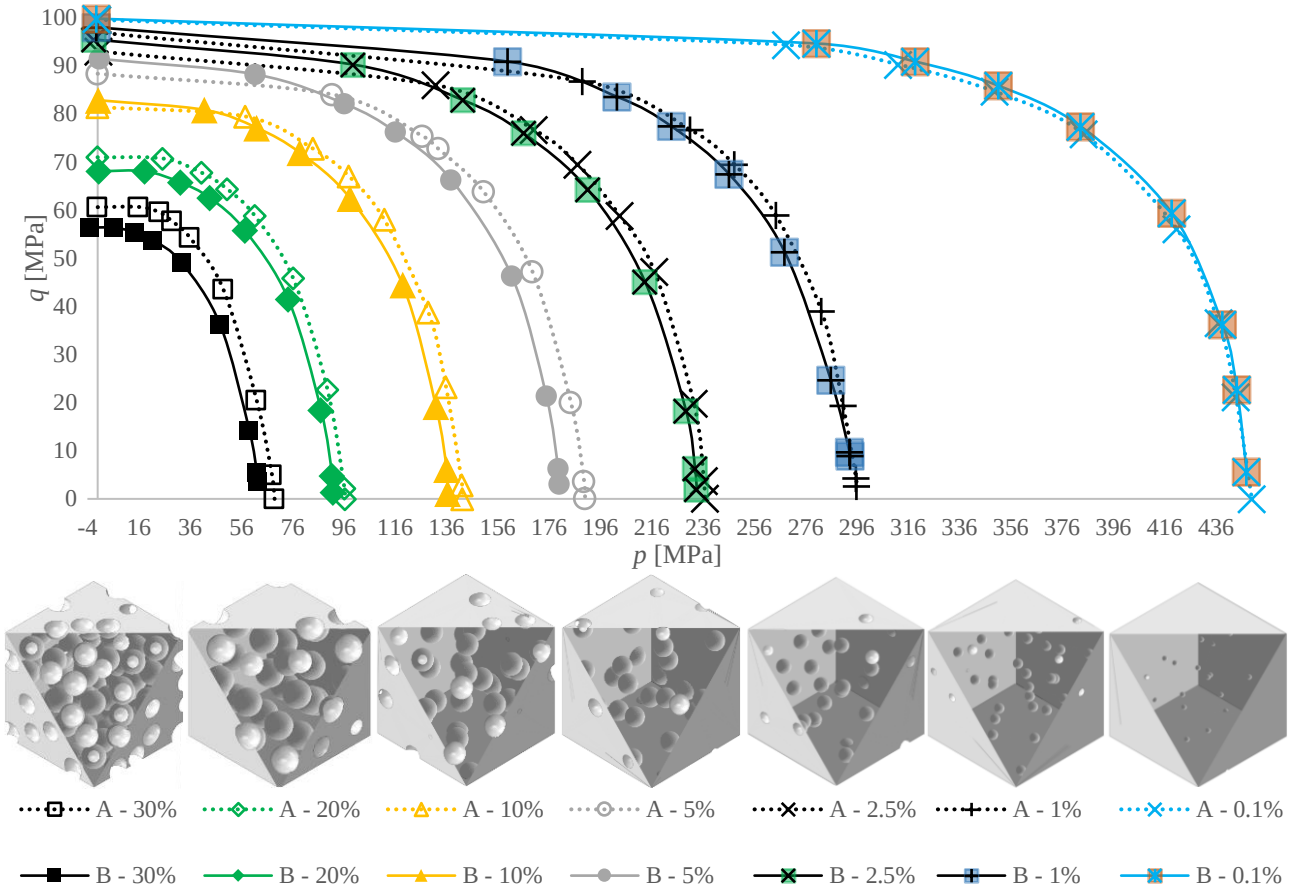

Figure 1 – Yield surface for computational homogenization model for multiple pores and single pores

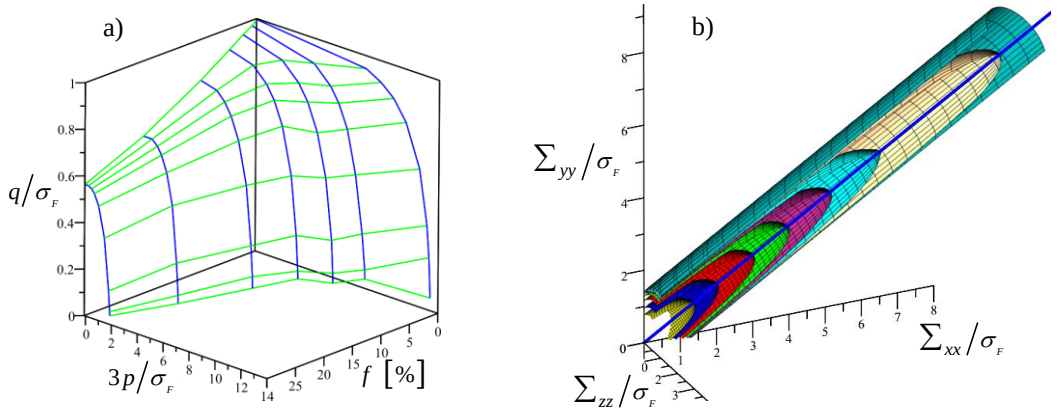

Figure 2 – Three-dimensional yield surface; a) in the *p-q-f* space, b) in the Σ_{xx}-Σ_{yy}-Σ_{zz} space

With the computed data, a curve fit was performed with aid of the Maple software, using the "CurveFitting" library with the "Interactive" routine, returning functions that represent the yield surface of each porosity level. These functions were plotted in the *q-p* space as $3p/\sigma_F$ on the abscissa axis and q/σ_F on the ordinate axis, further multiplied by cos(*r*) and sin(*r*), respectively, with *r* varying from zero 2π, that is, a rotation of the fit functions of the computed data from the yield surface was made to the positive side of the hydrostatic pressure. To represent the negative side, it was multiplied by -1. Thus, it is possible to obtain Fig. 2b). This figure shows the three-dimensional behavior in Σ_{xx}, Σ_{yy} and Σ_{zz} space of the yield surfaces calculated by computational homogenization and is an important illustration of the effects of the porosity levels into the macroscopic response where it is noted that for fully dense materials, the von Mises cylinder is recovered and for porous materials, an ellipse. For better visualization, the graph in Fig. 2b) was cut in the Σ_{xx}, Σ_{yy}, and Σ_{zz} planes at zero hydrostatic pressure and on the hydrostatic pressure axis.

Mesh Convergence

Figure 3 shows the mesh convergence study in a unit cell for the parameters f = 30% and N = 105 for von Mises and hydrostatic stress. Load case 9 (α=0, β=1 of Tab. 1) was chosen as an example and the discretization with the highest number of elements was taken as a reference and the response of the other discretization is related to the last calculated value of this discretization. The standard deviation for the stress components Σ_{xx}, Σ_{yy}, and Σ_{zz} was 2.87 MPa, 2.89 MPa and 2.54 MPa, respectively, and for von Mises and hydrostatic stress, 2.7 MPa and 2.76 MPa respectively. As seen in Fig. 3, the numerical error in relation to spatial discretization decreases monotonically and the difference between successive levels of refinement tends to zero.

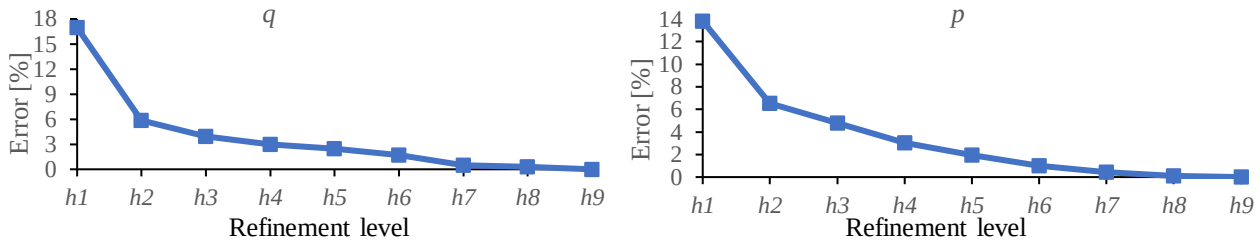

Figure 3 – Mesh convergence analysis of von Mises stress and hydrostatic

Based on this study, an average mesh density was chosen for the studies. Furthermore, based on the convergence study, the error for the discretization used is considered very small in relation to other influencing factors, such as the variation of microstructural geometry, as already observed by Fritzen et al. (2012).

Asymptotic Results

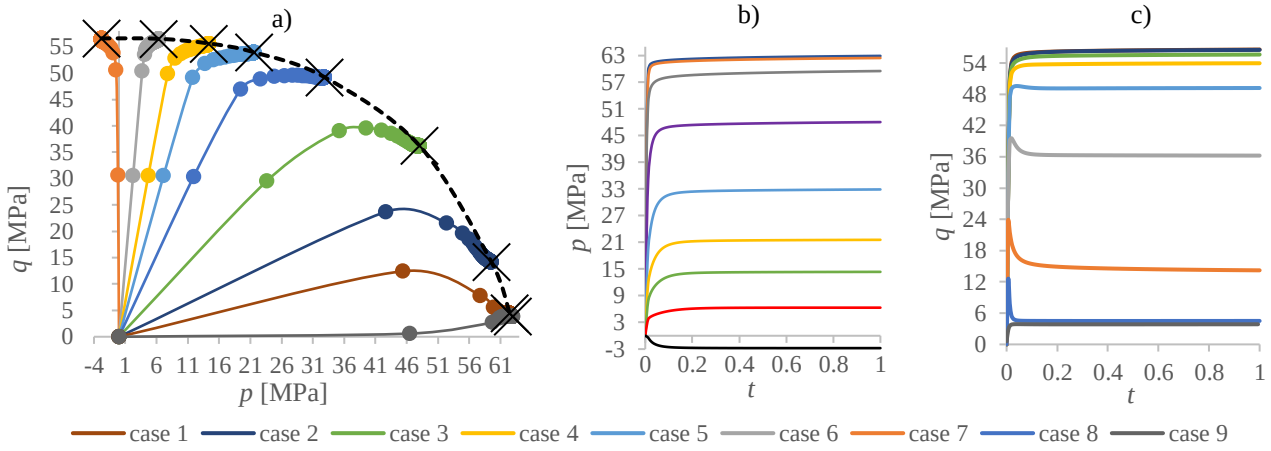

Figure 4 – RVE asymptotic behavior. a) *q- t*; b) *p-t*

The asymptotic behavior of porous microstructures was investigated using the Abaqus post-processing script written in Python language. By using the macroscopic stress (Eq. (1)) at the end of the simulation time (StepTime=1), it was found that all loading cases are tending to the asymptotic value, in the sense that the change in macroscopic stress tends to zero when the overall strain load is increased, as shown in Fig. 4b) and c). In Fig. 4b) and c), the time interval t between one increment ("FRAME") and another is 0.00625, totalizing 160 increments. Notice in Fig. 4c) that the hydrostatic pressure for the interval of $0 \leq t \leq 0.2$ (approximately) is not asymptotic. This can be seen with help of Fig. 4a) and b). Note that for some loading cases, there is only asymptotic behavior after t>0.2. This means that a total load around 3 times smaller could be used, with a time of $t \approx 0.4$, saving computational time.

In order to find out the significance of the asymptotic stress response obtained with respect to the loading history, the time history of the model simulation of 30% pore volume fraction is shown in Fig. 4a) along with the yield surface (dashed line). The dependence of hydrostatic pressure on the macroscopic yield response of the porous material is clearly visualized. The yielding points are obtained at the end of the simulations and are highlighted with an "×". In the particular choice of stress space, it was found that the simulations do not describe a straight line, but a rather complex non-proportional path, as already observed by Fritzen et al. (2012) and Khdir et al. (2014). Which could be a limitation of the method to evaluate the void growth under constant stress triaxiality. In contrast, the simulations using the Gurson and GTN models provide a loading history consisting of straight lines in the *q-p* space (constant stress triaxiality).

Representativeness

By analyzing the single pore models and the random microstructures shown in Fig. 1, it is noted that for small porosity a single pore in a reference cell seems to give a sufficiently close approximation to the ductile behavior of the examined random isotropic microstructures. This is not the case for larger volume fractions of voids. The asymptotic stress response of the microstructures examined for 30% pore volume fraction shows a deviation of 8.16% from the single pore model when related purely deviatoric (load 1 of Tab. 1). This also shows that for high porosity, a single pore model is not representative of a randomly distributed multiple pore model.

The von Mises and hydrostatic stress response are shown in red points in Fig. 5c) and d) to verify the influence of the representativeness on the set of microstructures one-size-fits-all and randomly distributed, created for porosity f = 30% and variable number of pores of N=1, 5, 21, 44, 70, 105, 126, 150, 162, 200. Note that the value of N=105 is close to the midline (dashed line). Of the 10 simulations with 10 different microstructures N=105 was chosen because it presents the smallest error associated with von Mises stress and hydrostatic as a function of the average of the 10 models, this is represented in Fig. 6. Despite a number of pores N=105 for a porosity level of 30%, it is noteworthy that not all voids are completely inside the RVE, some are less than half inside the RVE and these pores also account for N=150. These voids outside the RVE domain exist because they are randomly distributed (Mote3D (Richter, 2017)), but respecting the periodicity.

In the verification of the discrepancy between the construction of the randomness of the pores of the RVEs with the Mote3D (Richter, 2017) with N=105, it was found that the homogenized results for von Mises and hydrostatic stress were close to the calculated mean (dashed line) and are plotted as triangles in Fig. 5c) and d).

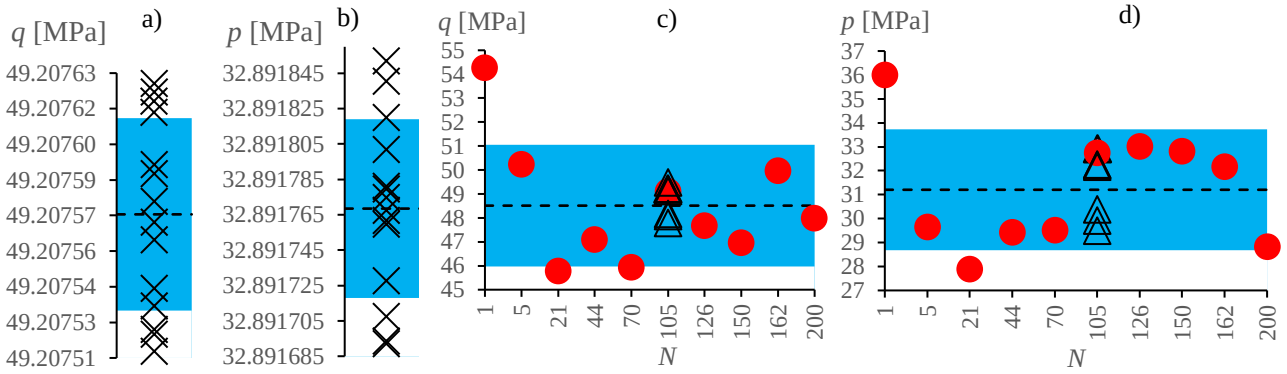

Figure 5 – Representativeness, a) different RVE scales for *q*, with N=105, b) different RVE scales for *p*, with *N*=105, c) different numbers of pores per RVE for *q*, d) different numbers of pores per RVE for *p*

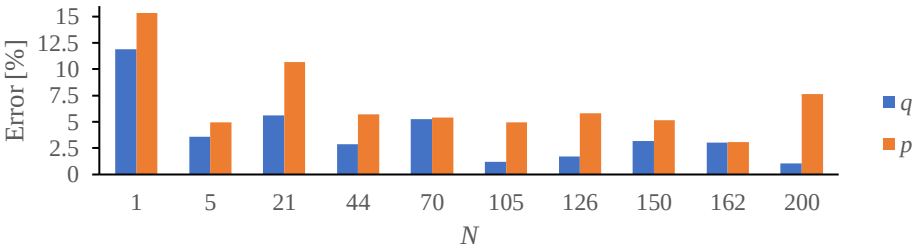

Figure 6 – Representativeness, error in relation to the average

To show that there is no length scale associated to the RVE size, other 14 microstructures were modeled with a scale ranging from 0.25 to 10 times of the RVE volume. The Figs. 5a) and b) show that the simulated RVEs do not vary as the length scale changes, where the standard deviation for q and p were respectively 0.000040 MPa and 0.000050 MPa. The 14 RVEs with different scales are plotted in ×, the standard deviation in blue and the mean as a dashed line. As expected for this type of analysis, when keeping the same mesh and just changing its size, the results are the same and the deviations between the analyzes performed are related to the numerical precision when scaling the volume, rather than an associated error to the homogenization method.

Within the realizations containing 105 voids, the mean deviation values of the 7 simulations represented by triangles in Figs. 5c) and d), are 1.26% of error for von Mises stress and 3.85% for hydrostatic stress. However, the standard deviation is 0.38% and 1.27% of error for von Mises stress and hydrostatic stress, respectively. All computed data is found within or near the blue area defined by the standard deviations. The computational results presented can be considered representative for the considered microstructure.

Original model Gurson and GTN

Figure 7 shows the comparison of the Gurson yield surface with the computational homogenization method for multiple pores. Note that the Gurson model overestimates the results, creating a larger surface than the computational method, it can be classified here as an upper bound. The data in Fig. 7 and Fig. 8 was extracted with the Porus Metal Plasticity package (Abaqus, 2022) in the Abaqus software.

Figure 8 shows the response for the GTN yield surface using parameters q_1, q_2, and q_3 of Eq. (4) of the reference Zuo et al. (1996) (Tab. 4) and presents a comparison of the computational homogenization model for all the cases of different porosities plotted on the same graph. Note that the GTN model does not overestimate the results like the original Gurson model. Compared to Gurson's classical model, the GTN model was closer to the results of computational homogenization.

The purpose of using the Abaqus Gurson and GTN models was to evaluate the loading history, but for reasons of brevity of text, it was not presented here. The difference from the loading history shown in Fig. 4 is that the Gurson and GTN models showed a constant triaxiality.

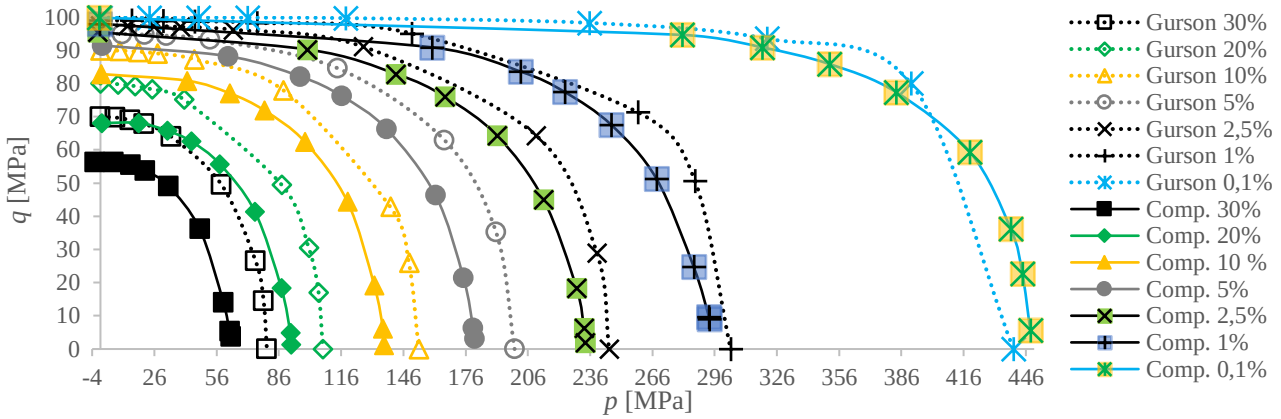

Figure 7 – Yield surface model Gurson and computational model

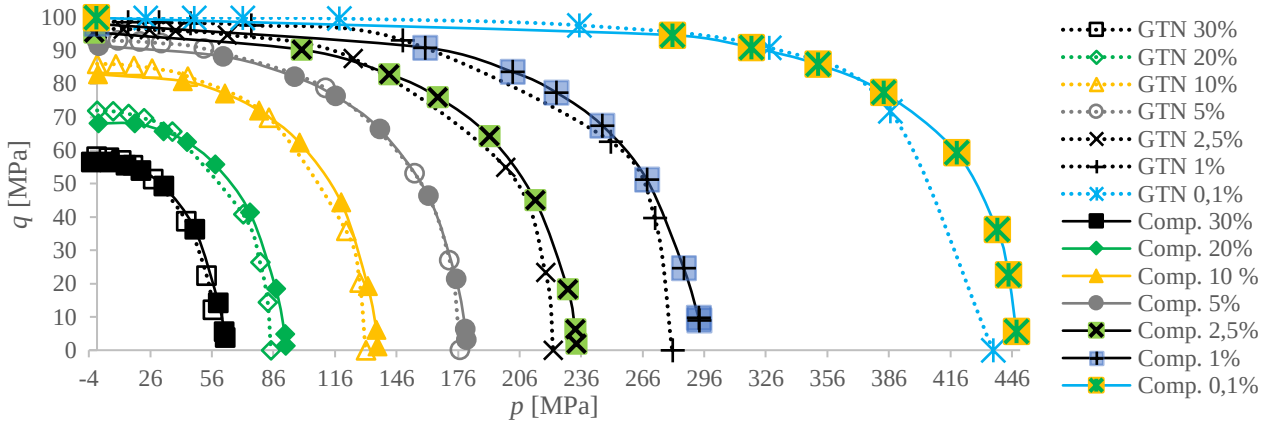

Figure 8 – Yield surface model GTN and computational model

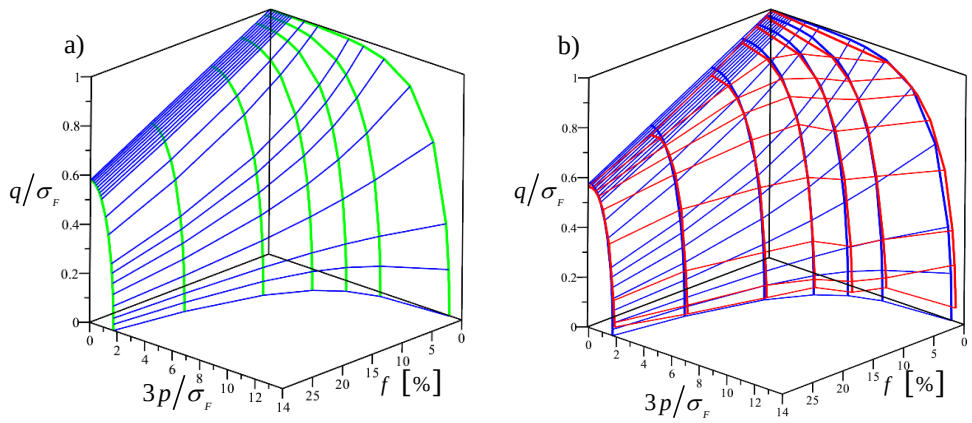

Figure 9 – Yield surface in the *p-q-f* space; a) GTN model, b) comparison, GTN in blue and computational homogenization in red

The graph presented in Fig. 9 (a) shows the yield surface in the *p-q-f* space, where the green curves are the yield surfaces for each porosity level and the blue curves represent the connections of the load cases of Tab. 2 evaluated between porosity levels. It is notable how the yield surface decreases with increasing porosity. It can be seen that for all porosity levels, the GTN model almost coincides with the yield surface of the computational homogenization model, as can be seen in the *p-q-f* space of Fig. 9b) (computational homogenization model in red).

CONCLUSIONS

In this work we numerically evaluate the pressure dependence of a homogenized yield surface of several porous microstructures, investigating different stress triaxiality ratios for different loading cases. The periodic microstructures were modeled with spherical and non-overlapping pores, randomly distributed. Still, single pore microstructures were evaluated for comparison purposes, showing that a single pore is representative of multiple pores only for a very low volume of pore fractions. To calculate the stress averages, a code in Python language was developed. The data were computed, and the yield surfaces of all cases were generated. The results were also compared with the yield surfaces of the Gurson and GTN models. It was noted that the Gurson model overestimates the results when compared to the numerical results. For the results of the GTN flow surface model, parameters from different researchers were used and it was found that q_1=1.4 is closer to the results of the computational homogenization of the present work. 20 different loading cases were proposed and considered to represent the yield surfaces in *p-q-f* space, generating sufficiently smooth yield surfaces. A RVE representativeness study was carried out to show that the RVEs employed are indeed representative. A mesh convergence study was also carried out, which shows that an RVE with approximately 300,000 second-order tetrahedral elements presents satisfactory results. A graph was presented in the *p-q-f* space that can be useful to interpret the flow behavior of materials sensitive to hydrostatic pressure for different levels of porosity, making interpolation between the levels of pores, it is possible to arrive at an estimate for other levels of porosity. Still, a graph was created in the Σ_{xx}, Σ_{yy}, and Σ_{zz} plane where the flow surfaces can be easily identified as a function of porosity, it is noticed that for dense materials, the von Mises cylinder is recovered.

REFERENCES

Abaqus, 2022. “Porous metal plasticity”. https://abaqus-docs.mit.edu/2017/English/SIMACAEMATRefMap/simamat-c-pormetalplas.htm.

Ahmed Obeidi, M., Uí Mhurchadha, S. M., Raghavendra, R., Conway, A., Souto, C., Tormey, D., Ahad, I. U., and Brabazon, D., 2021, “Comparison of the porosity and mechanical performance of 316L stainless steel manufactured on different laser powder bed fusion metal additive manufacturing machines”, Journal of Materials Research and Technology, Vol.13, pp. 2361-2374.

Besson, J., Berdin, C., Bugat, S., Feyel, F., Forest, S., and Pineau, A., 2004, “Local approach to fracture. Science de la matière”. Presse des Mines.

Binder C., A., Lenzi, I. C. M., Mocellin, P, R., and Becker, 2013, “Processo de Fabricação de um Corpo Poroso, por Metalurgia do Pó e Composição Metalúrgica de Materiais Particulados”. INPI RPI2235.

Drugan, W. J. and Willis, J. R., 1996, “A micromechanics-based nonlocal constitutive equation and estimates of representative volume element size for elastic composites”, Journal of the Mechanics of Solids, Vol. 44, pp. 497-524.

Dunand, M. and Mohr, D., 2011, “On the predictive capabilities of the shear modified Gurson and the modified Mohr-Coulomb fracture models over a wide range of stress triaxialities and Lode angles”, Journal of the Mechanics of Solids, Vol.59, pp. 1374-139.

Faleskog, J., Gao, X., and Shih, C. F., 1998, “Cell model for nonlinear fracture analysis-I. Micromechanics calibration”, International Journal of Fracture, Vol.89, pp. 355-373.

Fritzen, F., Forest, S., Böhlke, T., Kondo, D., and Kanit, T., 2012, “Computational homogenization of elasto-plastic porous metals”, International journal of plasticity, Vol.29, pp. 102-119.

Fritzen, F., Forest, S., Kondo, D., and Böhlke, T., 2013, “Computational homogenization of porous materials of Green type”, Computational Mechanics, Vol.52, pp. 121-134.

Green, R., 1972, “A plasticity theory for porous solids”, Journal of Mechanical Sciences, Vol.14, pp. 215-224.

Guedes, J. and Kikuchi, N., 1990, “Preprocessing and postprocessing for materials based on the homogenization method with adaptive finite element methods”, Computer methods in applied mechanics. Vol.83, pp. 143-198.

Gurson, A. L., 1977, “Continuum theory of ductile rupture by void nucleation and growth: Part I-Yield criteria and flow rules for porous ductile media”.

Huet, Chistion. 1990. "Application of variational concepts to size effects in elastic heterogeneous bodies". Journal of the Mechanics and Physics of Solids, Vol.38, 813-841.

Kanit, T., Forest, S., Galliet, I., Mounoury, V., e Jeulin, D., 2003, "Determination of the size of the representative volume element for random composites: statistical and numerical approach", International Journal of solids and structures, Vol.40, pp. 3647-3679.

Khdir, Y., Kanit, T., Zaïri, F., and Naït-Abdelaziz, M., 2013, "Computational homogenization of elastic-plastic composites", International journal of solids and structures, Vol.50, pp. 2829-2835.

Khdir, Y.-K., Kanit, T., Zaïri, F., and Naït-Abdelaziz, M., 2014, "Computational homogenization of plastic porous media with two populations of voids", Materials Science and Engineering: A, Vol.597, pp. 324-330.

Kim, J., Gao, X., and Srivatsan, T. S., 2004, "Modeling of void growth in ductile solids: effects of stress triaxiality and initial porosity", Engineering fracture mechanics, Vol.71, pp. 379-400.

Koplik, J. and Needleman, A., 1988, "Void growth and coalescence in porous plastic solids", International Journal of Solids and Structures, Vol. 24, pp. 835-853.

Kuhn, H. and Downey, C., 1971, "Deformation Characteristics and Plasticity Theory of Sintered Powder Metals", Int. J. Powder Mat., Vol.7.

McElwain, D. S., Roberts, A., and Wilkins, A., 2006, "Yield criterion of porous materials subjected to complex stress states", Acta materialia, Vol.54, pp. 1995-2002.

Nègre, P., Steglich, D., Brocks, W., and Koçak, M., 2003, "Numerical simulation of crack extension in aluminium welds", Computational Materials Science, Vol.28, pp. 723-731.

Nielsen, K. L. and Tvergaard, V., 2009, "Effect of a shear modified Gurson model on damage development in a FSW tensile specimen", International Journal of Solids and Structures, Vol.46, pp. 587-601.

Richter, H., 2017, "Mote3D: An open-source toolbox for modelling periodic random particulate microstructures", Modelling and Simulation in Materials Science and Engineering, Vol. 25.

Tvergaard, V., 1982, "On localization in ductile materials containing spherical voids", International Journal of fracture, Vol.18, pp. 237-252.

Tvergaard, V. and Needleman, 1984, "A. Analysis of the cup-cone fracture in a round tensile bar", Acta metallurgica, Vol.32, pp. 157-169.

Yan, Y., Sun, Q., Chen, J., and Pan, H., 2013, "The initiation and propagation of edge cracks of silicon steel during tandem cold rolling process based on the Gurson-Tvergaard-Needleman damage model", Journal of Materials Processing Technology, Vol.213, pp. 598-605.

Zaitsev, Y. and Wittmann, F., 1981, "Simulation of crack propagation and failure of concrete, Matériaux et Construction", Vol.14, pp. 357-365.

Zhang, Y. and Harding, J., 1990, "A numerical micromechanics analysis of the mechanical properties of a plain weave composite", Computers & Structures, Vol. 36, pp. 839-844.

Zhang, Z., Thaulow, C., and Ødegård, J., 2000, "A complete Gurson model approach for ductile fracture", Engineering Fracture Mechanics, Vol.67, pp. 155-168.

Zohdi, T. I. and Wriggers, P., 2004, "An introduction to computational micromechanics", Springer Science & Business Media. Vol.20.

Zuo, J., Lou, Z., and Kuang, Z., 1996, "A yield function for porous ductile materials", Engineering fracture mechanics, Vol.53, pp. 557-559.

RESPONSIBILITY NOTICE

The authors are the only parties responsible for the printed material included in this paper.

ACKNOWLEDGMENT

The author Rodrigo Rossi wishes to acknowledge the support of CNPq, Conselho Nacional de Desenvolvimento Científico e Tecnológico of Brazil, grant number 309430/2021-6, and of FAPERGS, Fundação de Amparo à Pesquisa do Estado do Rio Grande do Sul, grant number 19/2551-0001954-8-1. The author Tiago dos Santos wishes to acknowledge the support of FAPERGS, Fundação de Amparo à Pesquisa do Estado do Rio Grande do Sul, grant agreement 21/2551 − 0000744 − 3.